Mesua ferrea L. Seed Oil Based Amido-Amine Modified Nanoclay/Epoxy Nanocomposites

Gautam Das, Niranjan Karak

Department of Chemical Sciences, Advanced Polymer and Nanomaterial Laboratory, Tezpur University, Napaam, Sonitpur, Assam-784 028, India

Received 3 February 2011; accepted 19 July 2011
DOI 10.1002/app.35304
Published online 26 October 2011 in Wiley Online Library (wileyonlinelibrary.com).

ABSTRACT: Hydrophilic bentonite and organo-montmorillonite (OMMT) have been modified by using a vegetable oil based amido-amine compound. The modified nanoclays were characterized by using X-ray diffraction (XRD) and FTIR techniques. Increase in the basal spacing after the modification was observed in both the cases. Further, *Mesua ferrea* L. seed oil based sulfonated epoxy resin nanocomposites have been prepared by using these modified nanoclays [3 (w/w) of clay in each case]. The XRD, TEM, SEM, FTIR, and rheological studies confirmed the formation of partially exfoliated nanocomposites. The study also confirmed that hydrophilic bentonite is not suitable nanofiller for the system, though modified bentonite slightly improves the performance characteristics of the pristine polymer. Modified OMMT based nanocomposite shows significant improvement in tensile strength (~ 1.7 times), scratch hardness (~ 2 times), gloss (14 units), and thermal stability (18°C) compared to the pristine system. This nanocomposite also exhibit better performance than OMMT based analogous nanocomposite. © 2011 Wiley Periodicals, Inc. J Appl Polym Sci 124: 2403–2414, 2012

Key words: mechanical properties; organoclay; nanocomposites; renewable resources; thermal properties

INTRODUCTION

Nanoclays finds myriad of applications bestowed on their natural abundance and the propensity with which they can be chemically and physically modified to meet modern technological needs. Among the different types of clays, smectites are widely used by virtue of their high cation exchange capacity, excellent ability to swell, high platelet aspect ratio, and the ease with which their surfaces can be modified.[1,2]

The smectite clay with its rich intercalation and ion-exchange chemistry enables its organo-modification through the introduction of different organic cations or polymerization catalysts.[3,4] The formation of polymer nanocomposites by using this organo-modified nanoclay exhibits improve mechanical properties, barrier properties, thermal stability, resistance to swelling and fire, and ablation performance compared to the pristine polymer and the conventional composites.[5,6] These improvements are primarily as a consequence of the unique interfacial effects that result from the dispersion of the silicate nanolayers in the polymer matrix.

Correspondence to: N. Karak (karakniranjan@yahoo.com).
Contract grant sponsor: DRDO; contract grant number: ERIP/ER/0403490/M/01/962

The dispersion (intercalated or exfoliated structure) of clay mostly depends on thermodynamic compatibility between the different component present (polymer, clay, and organic modifier) in the system. Hence, for a favorable free energy of nanocomposite formation, a proper choice of the cationic organic modifier is necessary.[7]

Alkylammonium ions are mostly used for this purpose, although other "onium" salts can be used, such as sulfonium and phosphonium.[8–10] Depending on the functionality, packing density, and length of the organic modifiers, the organo-modified layered silicates (organoclays) can be engineered to optimize their compatibility with a given polymer.[7,11] The limited availability of commercial organoclays modified with ammonium ions (which are mostly petroleum based aliphatic nonpolar organics) provides the principal motivation for preparation of vegetable oil based polar organic modified nanoclays. This type of modification of montmorillonite may facilitate to control the final structure and end properties of polymer nanocomposites as well as in other applications.

The dictates of green chemistry for research to circumvent ecological challenges with concomitant optimized performance through maximal resource management have prompted the scientists to switch over to bio-based raw-materials.[12–16] These facts marshal in support of the use of *Mesua ferrea* L. seed oil [70% (w/w) oil content] as the raw material for

advanced material preparations. The fatty acid composition of the oil is as follows, it contains oleic acid (52.3%) and linoleic acid (22.3%) as unsaturated fatty acids and stearic acid (9.5%) and palmatic acid (15.9%) as saturated fatty acids. The literature reports on exploitation of this oil in the fields of medicine[17] and biodiesel[18] along with its use in the field of polymer.[19–22] But there is no report on the use of the fatty acid amido-amine of this oil in modification of nanoclay. The unique combination of the both polar and nonpolar part in the structure may be an apt choice for use of the amido-amine as modifier for nanoclay. The fatty acid amido-amine of *Mesua ferrea* L. seed oil may involve in H-bonding or ionic bonding with the thin platelets of nanoclay and thereby manifesting in self-assembly process to form a superhydrophobic surface. Conversely, the flexible alkyl groups tethered to the rigid platelet surface can offer higher degree of compatibility of the silicate layers with the polymers. Additionally, the presence of amine in the layer structure may catalyze the homopolymerization and crosslinking processes of the matrices like epoxy resin.

Epoxy resin is one of the most important engineering thermoset widely used in various applications like surface coatings and paints, electronics, composites, etc.[23] Sulfone based epoxy resin are known to exhibit superior performance than bisphenol-A based epoxy. Further, vegetable oil based sulfone epoxy has many added advantages as described in earlier report.[24] Hence, *Mesua ferrea* L. seed oil based sulfone epoxy is used as the matrix for the preparation of nanocomposites in the study.

Therefore, herein in this report, the modification of hydrophilic and organophilic nanoclay by using *Mesua ferrea* L. seed oil based fatty amido-amine was studied for the first time. The preparation, characterization, and properties evaluation of *Mesua ferrea* L. seed oil based sulfonated epoxy resin/modified nanoclay nanocomposites are also reported here. The comparisons were also made with respect to the nanocomposites obtained by using the penultimate nanoclay and the same matrix.

EXPERIMENTAL

Materials

Mesua ferrea L. (Nahar) seeds (Jamugurihat, Assam) were used for extraction of the oil. Epichlorohydrin, 1,6-diamino hexane (Merck, Mumbai, India) and bis(4-hydroxy phenyl) sulfone (Aldrich, Germany) were used as received. Bisphenol-A (BG, India) was used after purification by recrystallization from toluene. Montmorillonite [OMMT, $(Ca;Na)_{0:3}(Al;Mg)_2Si_4O_{10}(OH)_2.nH_2O$ with 25–30% (w/w) of octadecylammonium ions modified], (Nanoclay Nanomer® I.30E, Aldrich, Germany, CEC, cation exchange capacity 90 meqv/100 g) and inorganic bentonite [$(Na;K;Ca)_{0:3}(Al;Mg)_2Si_4O_{10}(OH)_2.nH_2O$, CEC 89 mqev/100 g] (Nanoclay Nanomer^R PGV, Aldrich, Germany) were used as received. All other reagents used in the present investigation were reagent grade.

Preparation of methyl ester of *Mesua ferrea L.* seed oil

The methyl ester of the oil was prepared as reported in the earlier published report.[20] Briefly, 25 g of oil in 50 mL super dry methanol and 0.5% sodium methoxide (with respect to the oil) were refluxed for 3 h in 250 mL round bottom flask under the nitrogen atmosphere. The content of flask were then cooled to room temperature and kept for overnight. The excess methanol was removed by distillation and the methyl esters were extracted by petroleum ether (bp 60–80°C) followed by washing with 15% aqueous NaCl solution and finally dried over anhydrous sodium sulfate. The methyl esters of the mixed fatty acids were purified from petroleum ether by distillation.

Preparation of *Mesua ferrea L.* seed oil based fatty amido-amine (AMNO)

Mesua ferrea L. seed oil based fatty amido-amine was obtained from the methyl ester of the oil by the following procedure. Methyl ester (0.0585 mol) and sodium methoxide [0.5% (w/w) as catalyst] were taken into a three-necked round bottom flask equipped with a condenser, a thermometer, and a nitrogen gas inlet. Then 0.064 mol of 1,6-diaminohexane was added to the reaction mixture slowly. The reaction was then continued at room temperature for 2 h followed by heating at (50–60)°C for 1 h with constant stirring. The product was purified by washing it with petroleum ether to remove any unreacted methyl ester followed by double distilled water for two to three times, and finally by extracting it with THF and distillation under vacuum. Further, it was kept in a vacuum oven at (35–40)°C for 24 h before use. The yield of the reaction was about 90–92%. The product is coded as AMNO (Scheme 1).

Preparation of diglycidyl ether bisphenol-S (sulfone) epoxy resin

Mesua ferrea L. seed based sulfone epoxy resin was prepared by similar method as reported earlier[24] with little modification. Briefly, monoglyceride of the oil (obtained by glycerolysis technique), epichlorohydrin, bisphenol-A (BPA), and bisphenol-S (BPS) were treated together by maintaining the mole ratio of 1 : 5 : 2 : 1 at (110 ± 5)°C for 14 h in slightly

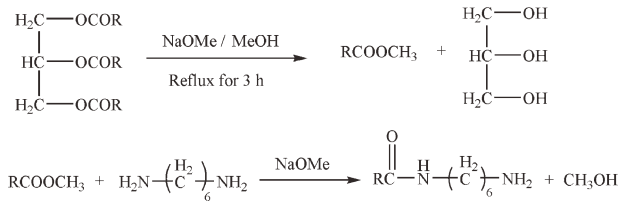

Scheme 1 Synthesis of fatty amido-amine from methyl ester of oil.

alkaline medium. The purified and dried product is coded as MBPSE.

Modification of organo-MMT (OMMT)

The dispersed organo montmorillonite (OMMT) in THF (10% v/w) and AMNO (30% by weight with respect to OMMT) was mixed together by magnetic stirrer under refluxed condition. It was continued for 3 h. The product was vacuum dried for overnight at 35–40°C. This product was coded as mOMMT.

Modification of hydrophilic bentonite (MMT)

In 50 mL of double distilled water, 0.5 g of clay was dispersed for 6 h at (50–60)°C using a magnetic stirrer with a reflux condenser. The salt of AMNO was prepared by neutralizing it using a 1*N* HCl for 12 h at (60–65)°C. The above two solutions were mixed together by magnetic stirring at 70°C. The heating was continued for 24 h. The resulting product was filtered and washed with distilled water until chloride ion is completely removed. The product was dried under vacuum for 24 h at 40°C. This product was coded as mMMT.

Fabrication of nanocomposites

At first the clay was vacuum dried at (35–45)°C for overnight. The nanocomposites were then prepared by incorporation of precalculated amount [3% (w/w) with respect to resin] of OMMT, mOMMT, mMMT and MMT with the MBPSE matrix. The components were mixed together at 80°C with constant mechanical stirring (at 1000 rpm) for about 2 h followed by sonication (pulse cycle 0.5 and amplitude 55–60%) for another 30 min. To avoid the rise of temperature during sonication, water bath was used to maintain the temperature at (25–30)°C. The dispersed nanoclay/resin system was degassed for 30 min under vacuum before further processing. The prepared nanocomposites were coded as ENMC1, ENMC2, ENMC3, and ENC for mOMMT, OMMT, mMMT, and MMT nanoclays, respectively.

Curing of the resin and nanocomposites

A homogenous mixture of the resin and the nanocomposites with 50 phr (parts per hundred gram with respect to epoxy resin) of poly(amido amine) hardener was prepared separately in a glass beaker at room temperature by stirring for about 20 min. A high vacuum was applied for about 15 min to remove any volatile generated during the mixing. The thin film of the mixture was then cast on a glass plate and kept for 2 h under ambient conditions. The plates were then heated at 100°C in a muffle furnace to determine the touch free time (minimum time, when no impression will appear on touching the film) and hard dry time (when no indentation on the film can be made by nail of the thumb) of the pristine resin and the nanocomposites. The mixtures were also uniformly spread on mild steel plates ($150 \times 50 \times 1.60$ mm^3), tin plates ($150 \times 50 \times 0.40$ mm^3) and glass plates ($75 \times 25 \times 1.75$ mm^3) for impact resistance, gloss and chemical resistance tests. The plates were cured at 100°C for specified period of time (Table I) and post cured at 150°C for 2 h.

Measurements

FTIR spectra of resin, OMMT, mOMMT, mMMT, MMT, and nanocomposites were recorded in FTIR spectroscopy (Impact-410, Nicolet) using KBr pellets. The viscosities of resin and the nanocomposites were measured by Rheometer of Model CVO100 (Malvern, UK) with a parallel plate geometry (plate diameter = 20 mm). The relationships between viscosity and time at constant stress (100 Pa) and single shear, viscosity against shear stress (20–200 Pa) and viscosity versus temperature (25–100°C) at constant stress of 20 Pa for the resin and the nanocomposites were determined from this study. The surface morphology of the samples was studied by JEOL scanning electron microscope of model JSM-6390LVSEM after platinum coating on the surface. Wide angle X-ray scattering (WAXS) studies were carried out using a powder diffractometer Rigaku X-ray diffractometer (Miniflex, UK) at room temperature (about 25°C), operated at 30 kV and 15 mA. The scanning rate used was 2.0 min^{-1} over the range of $2\theta = 0$–30° for

TABLE I
Drying Time and Viscosity of MBPSE and Nanocomposites

Sample code	Touch free time (min)	Hard dry time (min)	Viscosity (Pa s)	Swelling (%)
MBPSE	50	80	67.2	30
ENMC1	34	30	123	15
ENMC2	38	35	97	17
ENMC3	40	47	91.5	21
ENC	47	65	83.4	26

the above study. The distribution of nanoclay in the polymer matrix was studied by using a JEOL, JSM-100CX transmission electron microscope (TEM). Sample for TEM analysis was prepared by solvent casting method wherein very dilute solution of the sample was prepared in THF, the solution was sonicated in a water bath for 5 min, one or two drops of this solution was then placed on a copper grid, and the grid was then dried in a oven for 1–2 h, before further analysis.

The scratch hardness test (ASTM D5178/1991) of the cured films was carried out by using a scratch hardness tester (Sheen instrument, U.K). The front impact strength test was carried out by falling ball method using an impact tester (S.C. Dey & Co., Kolkata) with a maximum test height of 100 cm. In this test, a weight of 850 g is allowed to fall on the film coated on a mild steel plate from minimum to maximum falling height. The maximum height is taken as the impact resistance up to which the film is not damage.

The tensile strength and elongation at break (as per the ASTM D 412-51 T) of the samples were measured with the help of a Universal Testing Machine (UTM) of model Zwick Z010 (Germany) by using 10 kN load cell and at 40 mm/min jaw separation speed. The gloss characteristics of the cured films were found out by using mini glossmeter (Sheen instrument, U.K), over the resin and the nanocomposites coated mild steel plates at an angle of incidence of 60°.

Thermogravimetric (TG) analysis was carried out by Shimazdu TG 50 thermal analyzer using the nitrogen flow rate of 30 mL/min and at the heat rate of 10°C/min. The chemical resistance of the cured films was performed in different chemical environments. Glass plates coated with films were kept in 250 mL beakers containing 150 mL of different chemical media for 15 days and then the visual changes of the films were observed.

RESULTS AND DISCUSSIONS

Modification of nanoclay

The inherent incompatibility between the hydrophilic layered silicate and hydrophobic polymer matrix greatly hinders the reinforcement ability of the clay. Surface modification of hydrophilic clay was employed by long chain fatty amido-amine using cation exchange reaction. Further orgnanophilic clay was also cointercalated by the fatty amido-amine by employing simple intercalative technique. There are two main objectives for clay modification. The first one is to increase the basal spacing between clay layers by weakening the polar-polar interaction between adjacent layers, which is a prerequisite for polymer chains to intercalate into the clay galleries.

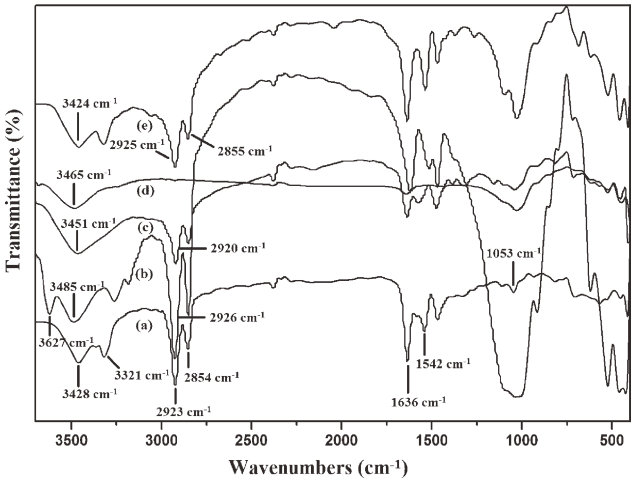

Figure 1 FTIR spectra of (a) AMNO, (b) OMMT, (c) mOMMT, (d) MMT, and (e) mMMT.

Whereas the second objective is to enhance the compatibility between polymer and clay, which provides a driving force for polymers to migrate into the silicate galleries. Preparation of organophilic clay and the property of polar organic surfactant play a crucial role in the formation of the structure and morphology of polymer nanocomposites.[25] The *Mesua ferrea* L. seed oil based amido-amine containing long hydrocarbon chains and polar groups can be effective in reducing the surface energy of the clay thereby improving the compatibility between the polymer and the layer silicates.

Characterization of modified nanoclay

FTIR analysis

The FTIR spectra of AMNO, OMMT, mOMMT, MMT, and mMMT are shown in Figure 1. The presence of amine group in the structure of AMNO was confirmed by the appearance of two weak absorption bands at around 3428–3312 cm^{-1}. The absorption band around 3428 cm^{-1} is due to the primary —*N*—H stretching vibrations. Whereas the absorption band around 3312 cm^{-1} is attributed to the secondary —*N*—H stretching vibration. Further, the band around 1636 cm^{-1} is primarily due to the stretching vibration of amide carbonyl of the fatty acid. Other characteristic bands observed in the spectra are 2923–2854 cm^{-1} (—CH_2 stretching), 1542 cm^{-1} (*N*—H bending), and 1053 cm^{-1} (C—N stretching). The spectrum of OMMT shows the presence of bands (cm^{-1}) at 3627 (associated to the stretching mode of the —OH group coordinated to Al cations), 3485 for —OH stretching, 2926 for —CH_2 stretching of modifying hydrocarbon, 3263 for —*N*—H stretching, 1619 for —OH bending, 1045–980 and 524–429 for oxide bands of metals (Al, Mg, Si, etc.) present in the clay.[23,26] After modification of OMMT by fatty

amido-amine (i.e., mOMMT) the —OH stretching vibration showed a shift of 34 cm^{-1}, while the —CH_2 stretching vibration showed a shift of 6 cm^{-1} only. A shift in the position of the —CH_2 absorption band from 2926 to 2920 cm^{-1} (asymmetric stretching) indicates an increase in the packing density for mOMMT.[11] These indicate that the modifying hydrocarbon of the fatty acids influences the arrangement of the octadecylammonium ion in the clay layers and thereby influencing the interlayer spacing. Further, in the spectra, the band for amide carbonyl stretching was also observed at 1638 cm^{-1} for the mOMMT, while the *N*—H deformation band shifts to 1577 cm^{-1}. This is indicative of the intercalation of the fatty amido-amine into the clay layers. In case of unmodified bentonite (MMT), the spectrum is quite similar to OMMT. Characteristics bands for the hydrophilic bentonite were observed at 3465 cm^{-1} (—OH stretching), 1640 cm^{-1} (—OH bending vibrations), 1032 cm^{-1} (Si—O or Mg—O stretching) and 520–424 cm^{-1} for oxide bands of metals (Al, Mg, Si, etc.). After modification for mMMT the —OH stretching frequency exhibits a red shift to 3424 cm^{-1}. This shift results from the H-bonding of the hydroxyl group of the clay with the amide carbonyl (—CONH) or secondary —NH group of the fatty amido ammonium ion. Further, the N^+H_3 ion may be involved with the ionic interaction with the surface oxygen resulting in the shift of the —OH absorption band with respect to the pristine clay.[25] In the spectrum of mMMT, appearance of additional bands (cm^{-1}) at 3314 (*N*—H stretching), 2925–2855 (CH_2 stretching), and 1538 (*N*—H deformations) confirms the modification.

X-ray diffraction (XRD) analysis

The basal spacing of the hydrophilic clay and the organophilic clay can be identified from the XRD spectra (Fig. 2). OMMT shows a basal reflection at 4.15° corresponding to the {001} plane, this results to a basal spacing of about 6.4 nm. However, the surface modified OMMT by AMNO results in splitting of the peak into two. One peak appears at 2° corresponding to a basal spacing of about 10 nm, while other peak was seen in the spectrum at about 5.9°.[27] This may be due to the presence of two different components in the organoclay. The intercalation of the clay by AMNO further increases the interlayer spacing. Consequently, some parts of the organic amine may squeeze out of the interlayer, and shift the peak to the right.

The diffraction patterns of MMT and mMMT are shown in Figure 2. It can be seen from the figure that sharp peaks around 6.15° (*d*-spacing of about 3.6 nm) for hydrophilic bentonite and around 5.1° (*d*-spacing value is ~ 4.7 nm) for AMNO modified

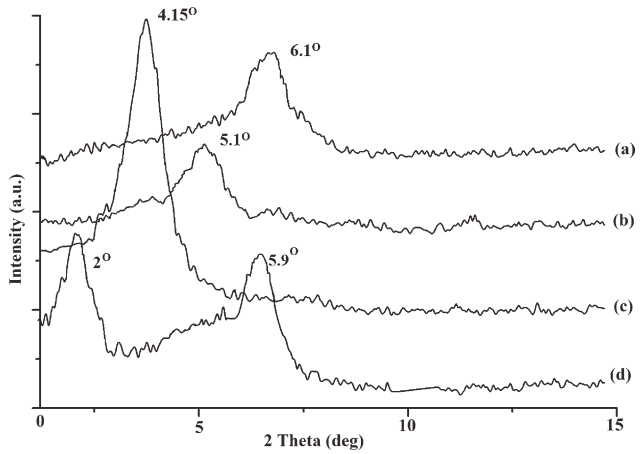

Figure 2 XRD patterns for of (a) MMT, (b) mMMT, (c) OMMT, and (d) mOMMT.

bentonite were observed. These results indicate that the modification is not sufficient to increase the inter layers spacing of the clay, significantly. However, the above results confirmed the fatty amido ammonium ion could modify the hydrophilic bentonite by cation exchange technique.

Thus higher basal spacing of mOMMT compared to mMMT may be attributed to the presence of the octadecyl ammonium ion in the clay galleries and also due to the use of proper modification methodology. This aids to the further expansion of the clay galleries by insertion of the fatty amido-amine. The presence of more number of functional group provides a greater degree of interaction; also, the long chains surfactant tethered away from the surface push the clay layers apart.

Nanocomposites preparation

The nanocomposites were prepared here essentially by *ex situ* technique. Fundamentally, it involves dispersion of the modified as well as unmodified clay into the epoxy matrix. Under the applied conditions delamination of the modified clay into individual silicate layer occurs, which ultimately become dispersed within the epoxy matrix. The separation of silicates into individual layer occurs by heating the clay and epoxy resin at 80°C, followed by sonication, addition of curing agent, and curing of the network at a prescribed set of temperatures. Initially, the epoxy resin and the clay were mixed mechanically at 80°C to facilitate the process, as the viscosity of the resin is low at that temperature. Further the mixing by ultrasonication helps in intercalation of the clay layers by penetration of the polymer chains to obtain the desired nanocomposite. Further the presence of alkylammonium ion in the gallery space may catalyze epoxy homopolymerization as well as crosslinking reactions.[28,29] This causes the clay layers

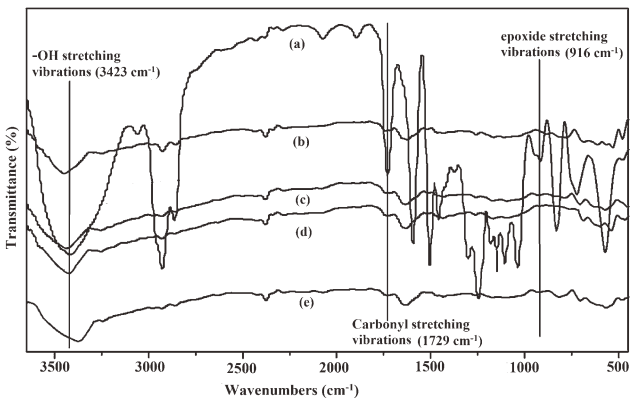

Figure 3 FTIR spectra of (a) MBPSE, (b) ENMC1, (c) ENMC2, (d) ENMC3, and (e) ENC.

to move further apart from each other. The driving force for the intercalation/exfoliation process is believed to be the high surface energy of the clay, which results in diffusion of polar species such as epoxy molecules between the layers. However, in the absence of polymerization, the system would reach a thermodynamic equilibrium and the layers could not be separated further. Since epoxy molecules reacts in the proposed polymerization process, they lower the polarity of clay and displace the equilibrium. Consequently, new polar epoxy molecules are driven between the layers to restore the equilibrium.[29,30] As this process proceeds further, more polymer molecules are driven between the clay layers to increase separation between the layers. For unmodified clay the hydrophilic character and the confined layer spacing prevents the diffusion of the epoxy chains. Thus, the high aspect ratio of clay in a delaminated structure offers an extensive filler-matrix contact, which may improve thermal, physical, and mechanical properties at low loading of organoclay.

Characterization of nanocomposites

FTIR analysis

The FTIR spectrum of MBPSE, ENMC1, ENMC2, ENMC3, and ENC are shown in Figure 3. Some of the characteristics absorption bands (cm^{-1}) for MBPSE are: 3423 (—OH), 3050 (aromatic C—H stretching), 1729 (C=O of the triglyceride esters), 1593 (C=C), 1300 and 1149 (for sulfone group), 1246 and 1106 (for C—O—C stretching vibrations), and 916 (for oxirane ring).[31] For the nanocomposites the interactions of the clay with the matrix can be understood from Figure 3. The —OH stretching vibrations in all the nanocomposites showed significant shifts. The band was shifted from 3423 to 3436 cm^{-1} for ENMC1, to 3433 cm^{-1} for ENMC2, to 3428 cm^{-1} for ENMC3 and to 3408 cm^{-1} for ENC. The observed shifts indicate the interactions of the clay with the MBPSE matrix through H-bonding. The disappearance of the peak for the epoxy ring around 916 cm^{-1} in all the nanocomposites indicates the completion of the oxide-ring opening reaction of epoxy rings of MBPSE in the presence of amine group of the poly(amido amine) hardener.

XRD analysis

The XRD pattern of all the nanocomposites shows no basal spacing corresponding to {001} plane in the diffractographs (Fig. 4) except for ENC (small peak at around 5.9). However, a broad peak in case of the nanocomposites was observed around 19.9°, which is due to the amorphous nature of the sulfone based epoxy resin. The results indicate that the clay layers may be exfoliated in the matrix. The increase of basal spacing in case of mOMMT helps the epoxy resin chains to intercalate by using the cointercalated OMMT. Upon intercalation of the OMMT by AMNO, the gallery cations reorient from their initial monolayer, lateral bilayer, or inclined paraffin structure to a more perpendicular orientation.[11] The basal spacings suggest that an all *trans* configuration might be adopted by the alkylammonium chain. A related reorientation of alkyl ammonium ions has been observed previously for ε-caprolactam intercalated clay intermediates formed in the preparation of Nylon-6-exfoliated clay nanocomposites.[32] Thus, the ability of the onium ion chains to reorient into a vertical position to optimize solvation interactions with the epoxy chains may achieve better layer separation upon intragallery polymerization in the nanocomposites.

Morphology of the nanocomposites

Figure 5 shows the SEM micrographs of the surfaces corresponding to ENMC1, ENMC2, ENMC3, and ENC nanocomposites. From the images, it can be seen that there is uniform distribution of the clay

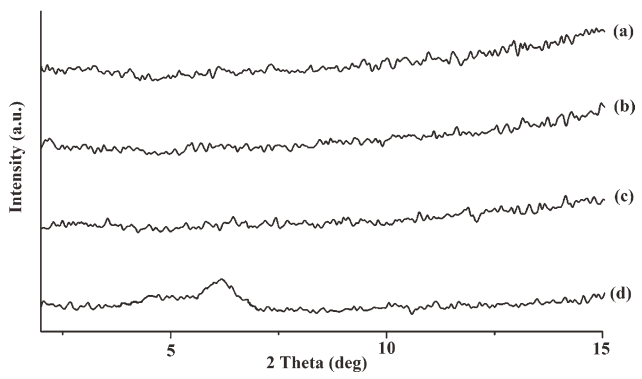

Figure 4 XRD patterns for of (a) ENMC1, (b) ENMC2, (c) ENMC3, and (d) ENC.

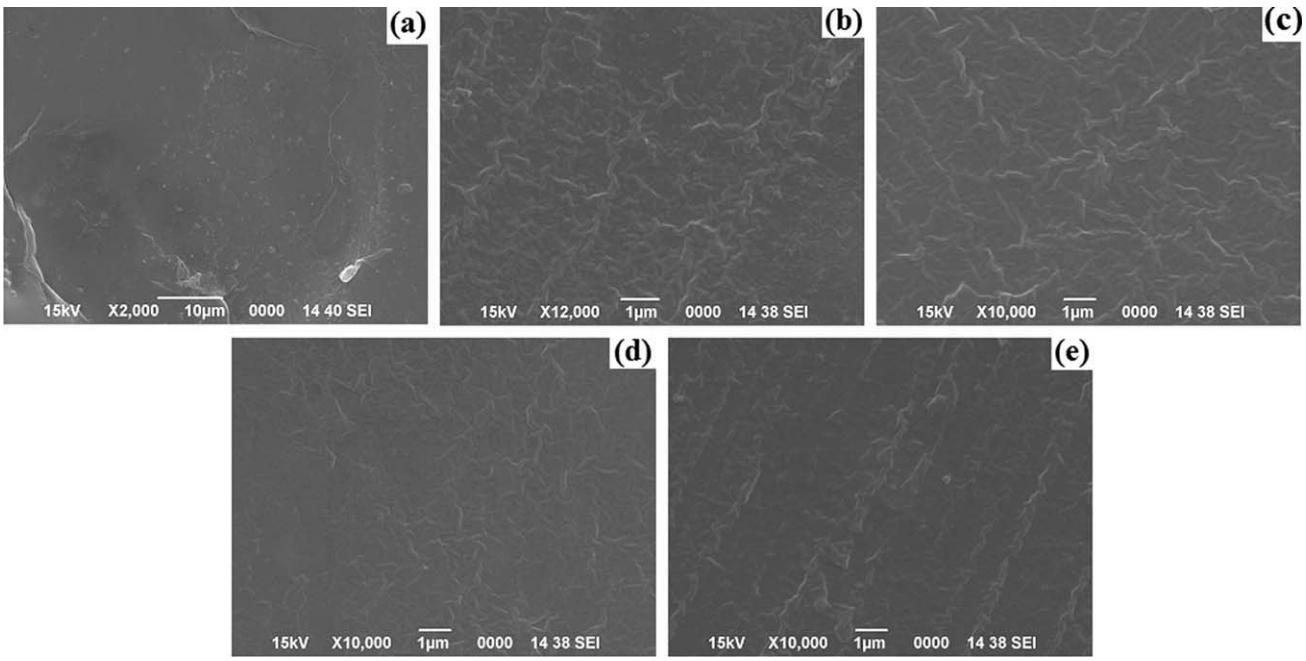

Figure 5 Representative SEM micrographs for (a) MBPSE, (b) ENMC1, (c) ENMC2, (d) ENMC3, and (e) ENC.

layers in the polymer matrix. ENMC1 shows the best dispersion of the clay in the matrix among the studied nanocomposites. The clay layers were delaminated in the matrix. These evenly distributed layers in the matrix would then interlock and entangle with the polymer chains. Therefore, the nanoclay present inside the epoxy acted like grid lines.[33,34]

However, it is not justified to conclude about the exact state of structure of the nanoclay layers that is exfoliated or not in the matrix just from XRD and SEM analyses. TEM analysis is necessary to support the structure of the nanocomposites. Figure 6 shows representative TEM micrographs of ENMC1 and ENMC3. The visibly dark lines in the figure correspond to the silicate nanolayers. A good dispersion of the clay platelets was achieved in case of ENMC1. Layer spacing of clay in the nanocomposites increases, wherein in some cases exfoliated structures were obtained. Thus, coexistence of both partly intercalated and exfoliated clay layers can be visualized in the epoxy matrix (Fig. 6).

The formation of partially exfoliated clay nanocomposites is dependent on the nature of the alkylammonium exchanged clays. The presence of longer linear alkyl chains of *Mesua ferrea* L. seed oil facilitates the formation of partially exfoliated nanocomposite. In the case of AMNO modified bentonite, the hydrophobicity of the galleries is relatively low,

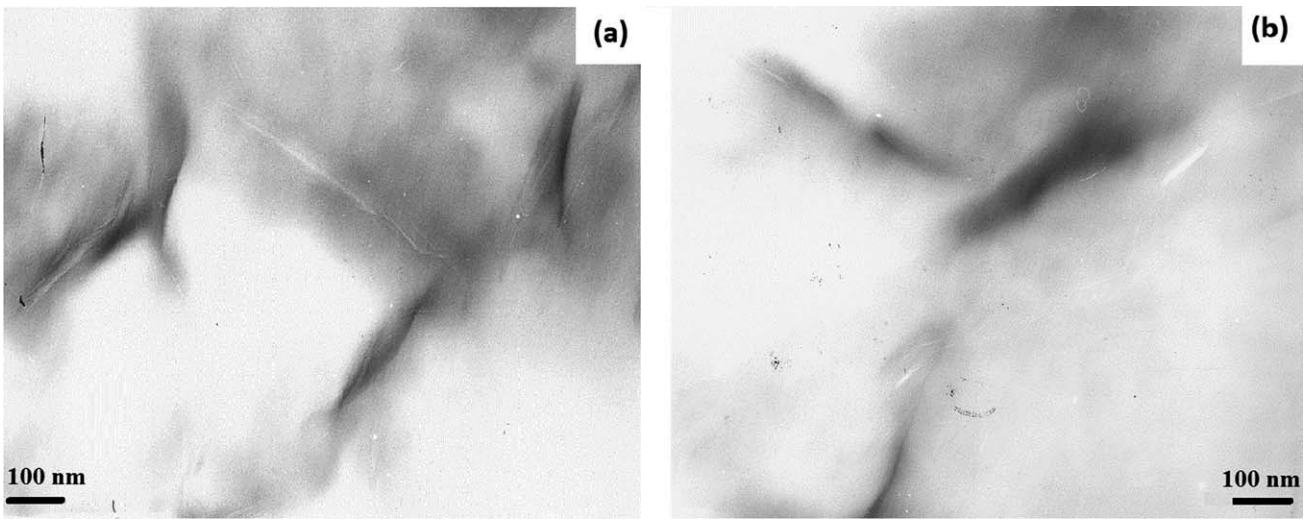

Figure 6 Representative TEM micrographs for (a) ENMC1 and (b) ENMC3.

and the amount of intercalated epoxide is insufficient to achieve exfoliation. Therefore, only a portion of the clay is delaminated as evident from the TEM micrographs (Fig. 6). Inorganic bentonite is hydrophilic and not readily swelled by epoxy monomers, making intragallery polymerization impossible. Therefore, a conventional type phase-separated composite was formed.

Rheological behaviors of MBPSE and its nanocomposites

The rheological characteristics of the resin and the nanocomposites were studied for variation of viscosity against time, shear stress and temperature. Table I indicates that there is a substantial increase in the viscosity for the nanocomposites, but still the nanocomposites exhibit Newtonian like flow behavior [Fig. 7(a)]. ENMC1 exhibits the highest viscosity. The enhanced viscosity is mainly attributed to the improved nanoscaled structure of clay tactoids, indicating that presence of AMNO is propitious to the well dispersion of clay. Consequently, the high surface functionality of clay interacts with the functional groups of MBPSE (epoxy or ester or hydroxyl). However, ENC shows the lowest viscosity indicating the presence of insignificant interaction between the clay layers agglomerates and the matrix.

The shear viscosity is not affected significantly with the increase of shear stress (20–200 Pa) [Fig. 7(b)]. The large surface area of the nanoclay can significantly interact with the matrix and consequently slows down the movement of the polymer chains due to greater interfacial adhesion. This prevents the preferential orientation and alignment of the silicate layers and the polymer chains to the direction of the flow.[35]

The variation of viscosity of MBPSE and its nanocomposites against temperature is shown in Figure 7(c). The temperature sensitivity of the shear viscosity has strong effect on the choice of processing conditions. As shown in Figure 7(c), viscosities of pure MBPSE and nanocomposite decrease with the increase of temperature in the range of 25–100°C at shear stress of 20 Pa. With the increase in temperature when shear force is applied, the interaction between the matrix and the filler decreases. As a result, the shear flow can induce an increase of distance between filler particles or between the filler and resin matrix, resulting in the destruction of the secondary bonds. Consequently, the array of particles becomes directional and the viscosity decreases.[36]

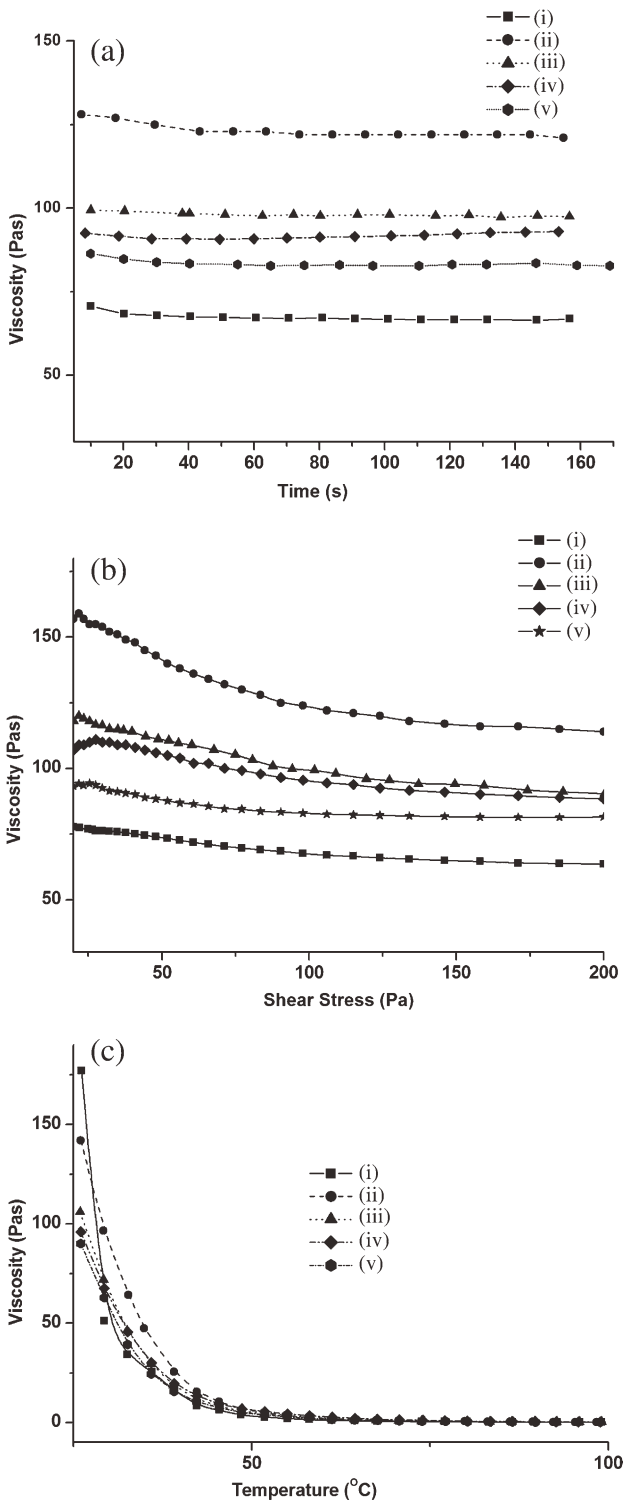

Figure 7 Variation of viscosity against (a) time at constant stress under isothermal condition, (b) viscosity against table of shear stress, and (c) viscosity against temperature under constant stress for (i) MBPSE, (ii) ENMC1, (iii) ENMC2, (iv) ENMC3, and (v) ENC, respectively.

Curing studies of nanocomposites

As can be seen from the FTIR spectra (Fig. 3) the intensity of the band for the epoxide ring in the nanocomposites almost disappears. This is indicative of the ring opening of the epoxide ring under the influence of the amine group of the hardener (i.e., crosslinking). The subsequent reaction of the

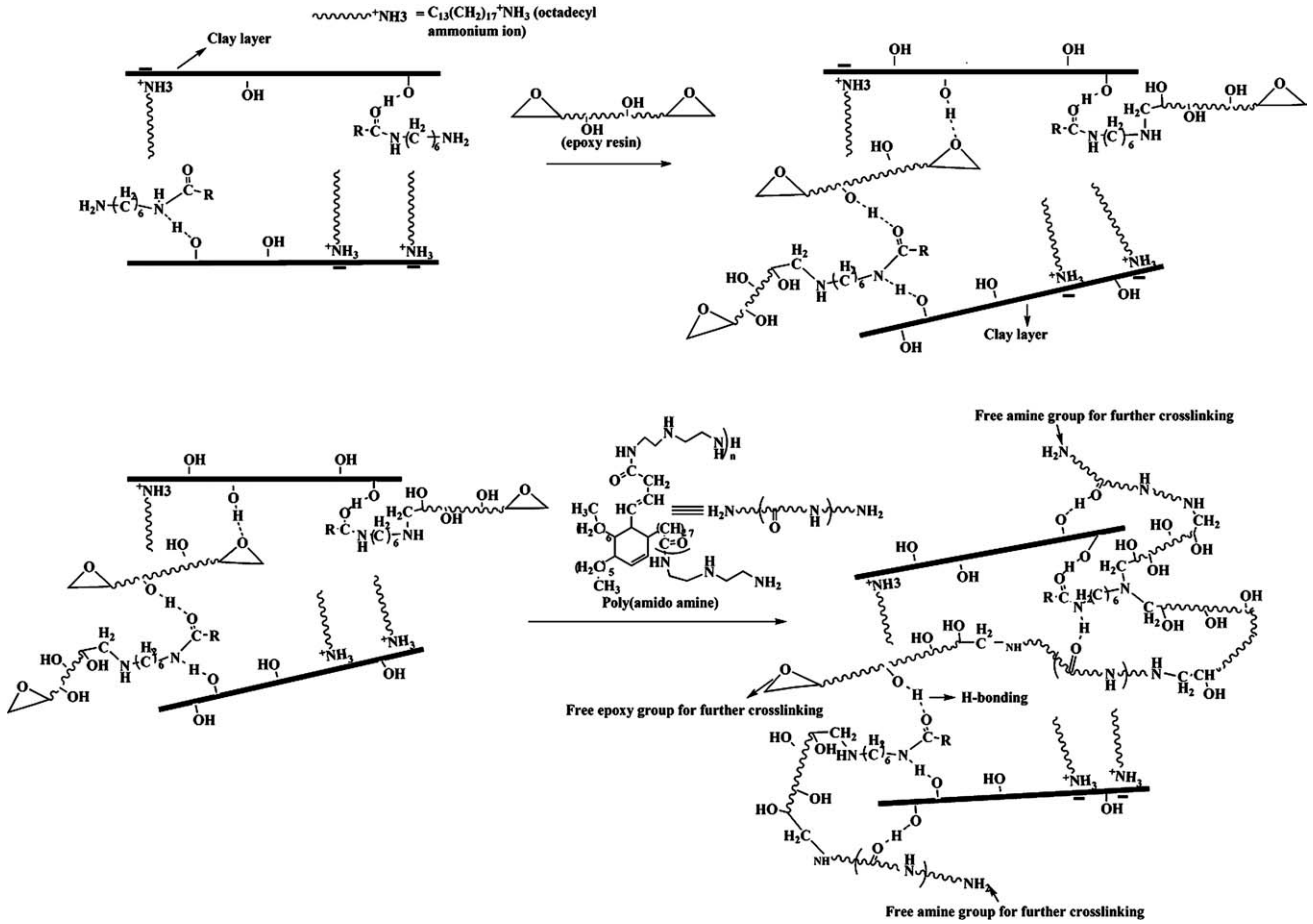

Scheme 2 Probable mechanism for interaction of clay, epoxy matrix, and epoxy with hardener.

hardener with the epoxy resin leads to a three dimensional crosslink network. As reported, the presence of hydroxyl groups has a catalytic affect on the curing of the epoxy resin.[11] Consequently, the hydroxyl groups of the clay synergistically decrease the curing rate of the epoxy resin. From Table I, it can be seen that ENMC1 took the lowest and the pristine took the highest time for curing. The mechanisms for this increase rate might involve hydrogen transfer from the donor to the epoxy, or hydrogen bonding of both the epoxy and the amine (Scheme 2). These long-chain alkylammonium exchanged montmorillonites cointercalated by AMNO provides a hydrophobic environment for the hardener to migrate into the clay interlayer region. Under the curing conditions, more epoxy and hardener penetrate the gallery space and intragallery polymerization can occur at a rate that is comparable to extragallery polymerization. However, considerable interaction of the hydroxyl containing material with the reactants may accelerate the epoxy/diamine curing in all the cases.

Performance studies of MBPSE and nanocomposites

The tensile strength shows an increase in value for ENMC1 compared to the pristine system (Table II). The efficiency of clay in the reinforcement of polymer systems is dependent on their degree of dispersion in the organic medium. Better, the dispersion of the clay layers in the matrix, greater is the surface area available for interaction with the polymer matrix, higher will be the strength. The improved tensile strength of ENMC1 can be attributed to good dispersion of the clay in the matrix. The presence of high functionality in mOMMT increases the interactions between the silicate layers and the epoxy matrix by hydrogen bonding or dipolar interactions. This subsequently increases the tensile strength of

TABLE II
Performance Characteristics of MBPSE and Its Nanocomposites

Sample code	MBPSE	ENMC1	ENMC2	ENMC3	ENC
Tensile strength (MPa)	6	10	8.2	7.2	4
Elongation at break (%)	95	97	96	95	85
Impact resistance (cm)	100	100	100	100	90
Gloss (60°)	60	74	70	64	57
Scratch resistance (Kg)	3.4	6.2	5.3	4.7	3.5

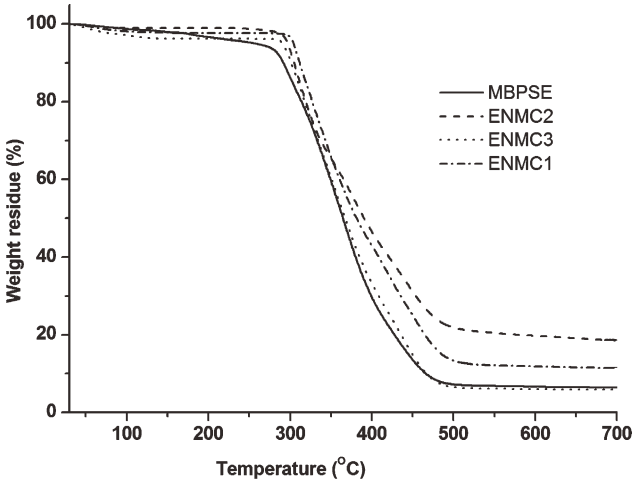

Figure 8 TGA thermograms of (a) MBPSE, (b) ENC, (c) ENMC3, (d) ENMC2, and (e) ENMC1.

the ENMC1.[37] ENMC2 exhibits higher tensile strength than ENMC3. The onium ion of the octadecyl amine has better intercalation ability than onium ion of AMNO. As seen from the XRD studies, mMMT has lower interlayer spacing compared to OMMT. Thus, the interaction of OMMT with the epoxy chains is more than mMMT with epoxy matrix. As a result, ENMC2 has better interfacial reinforcing ability that leads to greater load bearing capability compared to ENMC3. However, ENC has tensile strength lower than the pristine polymer. This reduction in tensile strength is attributed to the stress concentration, which arises by the agglomeration of clay. The elongation at break remains almost unaffected in all the cases, though a slight increase was observed in the case of ENMC1. The presence of long hydrocarbon chains and the internal bond strength rather than crosslinking density aids to the increase in elongation value. Elongation is a property influenced more seriously by chain breakage than chain slippage.[38] For ENMC1 the increase in scratch hardness may be attributed to the better dispersion of the clay in the matrix.[39] In other words, the gap between layers widening due to the AMNO modification of OMMT, the amount of epoxy inserted between layers also increases. This results in high interfacial adhesion between clay and the MBPSE matrix. Thus, the uniformly distributed clay layers (as seen from SEM images) in the matrix with large surface areas would alter the local stress of surrounding matrix. This effective crack deflection by the clay platelets thereby increases the toughness of the matrix.[40,41] This altogether results in a tough surface that becomes more difficult for making any penetration or indentation. The scratch hardness of ENC remains almost same as of the pristine polymer and the presence of agglomerated structure of the nanofiller results in low scratch hardness compared to other nanocomposites system. The impact strength for all the nanocomposites including pristine polymer reached the maximum limit of the used instrument (maximum height of 100 cm). These results indicate that as such there is no deterioration of impact resistance by the formation of nanocomposites.

The gloss characteristic of the nanocomposites has been found to increase significantly for ENMC1, ENMC2, and ENMC3. The improved gloss characteristics of the film can be correlated to the good crosslinking of the cured films (as supported by swelling data, Table I), which results in a smooth surface. As large amount of light is being reflected from the surface due to the smooth texture, so the gloss value increases with the clay content in this case (Table I).

Thermal properties

The thermogravimetric profiles of pure MBPSE and its nanocomposites with 3% (w/w) clay contents are shown in Figure 8. It can be seen that the initial decomposition of MBPSE occurs at 282°C, while for ENMC1, ENMC2, ENMC3, and ENC the decomposition occurs at 301, 296, 291, and 285°C, respectively, (Table III). All the systems exhibited a one-step degradation pattern. The presence of sulfone linkage due to its greater heat stability than the carbon–carbon, linkage improves the thermal stability of the MBPSE matrix.[41] Also, the presence of thermostable aromatic moieties results in increase in degradation temperature. These moieties have high rigidity and high steric hindrance to molecular mobility; consequently result in increase in the degradation temperature. The degradation of the epoxy network occurs by the elimination of water molecules, which may result in the formation of C—C unsaturations. The C—O bond in β-positions with respect to these unsaturations becomes the weakest linkage. They ultimately break downs to give fragments small enough to volatize at such high temperature. The extensive breakdown of the epoxy network occurs with the progressive increase in temperature. At higher temperature, the aromatic carbon bonds of

TABLE III
Thermal Degradation Pattern for MBPSE and Nanocomposites

Samples	Initial degradation temperature (T_0), °C	Peak temperature (T_{max}), °C	End temperature (T_f), °C
MBPSE	282	332	481
ENMC1	301	356	489
ENMC2	296	337	484
ENMC3	291	334	470
ENC	285	320	466

the bisphenol-A ring may break down leading to volatilization.

As evident from Figure 8, there is a good improvement in the thermal stability of the resin on the incorporation of nanoclay. However, there were no significant differences between peak temperatures of pristine system and the nanocomposites. The use of AMNO in OMMT probably reduces the hydrophilicity of the clay by reducing the cohesion between the stacks thereby prompting more amounts of polymer chains to enter into the galleries. This results in better dispersion of the clay in the matrix. Consequently, the well dispersed clay (with inorganic phases like SiO_2, Al_2O_3, and MgO) with high thermal stability and high barrier properties can prevent the heat from transmitting quickly into the bulk of the material and can limit the continuous decomposition. The crosslinking of the epoxy with the hardener results in a more thermally stable structure. Moreover, the clay layers assist in the formation of char after thermal decomposition that could also enhance the overall thermal stability of the system.[42]

Chemical resistance studies

The ENMC1 shows good chemical resistance over the pristine polymer (Table IV). The good dispersion of the clay with good interaction with the matrix effectively enhances the chemical resistance. The good chemical resistance of ENMC1 indicates improvement in the barrier properties. The well-dispersed clay layers in the matrix provides a torturous diffusion pathway for the ions or moisture, this significantly increases the time of their diffusion, which affects the chemical resistance. ENMC2 shows better diffusion properties than ENMC3, and consequently shows better chemical resistance. The pristine polymer shows poor alkali resistance, may be due to the presence of ester groups of the fatty acid that undergoes hydrolysis. The pristine polymer shows absorption of solvent (ethanol) and water. The absorption moisture of the epoxy network may be due to the presence of polar group in the network. The absorption of moisture was not significantly affected by nanocomposites formation. However, the ENMC1 shows low absorption of moisture.

TABLE IV
Chemical Resistance of MBPSE and Nanocomposites in Different Media

Sample code	Aq. NaOH (0.5%)	Aq. HCl (10%)	Aq. NaCl (10%)	Distilled Water	Ethanol (20%)
MBPSE	P	O	G	G	G
ENMC1	E	P	E	E	E
ENMC2	E	G	G	E	E
ENMC3	G	G	G	O	G
ENC	O	P	O	G	G

P, poor; O, peeled out; G, good; E, excellent.

TABLE V
Flame Retardancy of MBPSE and Nanocomposites

Samples	LOI value	UL94
MBPSE	28.4	V2
ENMC1	35	V1
ENMC2	33	V1
ENMC3	30.5	V1
ENC	29.5	V2

Flame retardancy

The flame retardancy has been found to be increased by formation of nanocomposites (Table V) of the epoxy matrix. Among the studied nanocomposites, the highest enhancement both in LOI value and UL94 ratings was observed for ENMC1 compared to the pristine system. This increase in the flame retardancy results from the good dispersion of the nanoclay in the matrix compared to other systems. The improvement in LOI value and UL94 rating for EMNC1 is due to the formation of a more efficient barrier to impede mass and heat transfer by the well-dispersed clay layers. The low improvement of flame retardancy in case of ENC is attributed to the poor dispersion of the clay. This results an ineffective barrier, which could not prevent the burning process and thereby low LOI value was observed.[43]

CONCLUSIONS

From this study it can be concluded that *Mesua ferrea* L. seed oil based fatty amido-amine is used for the first time as an effective modifier for OMMT to improve compatibility with the epoxy matrix. Further, the hydrophilic clay was intercalated with ammonium salt of AMNO by cation exchange reaction. The modified clay exhibited higher basal spacing compared to pristine clay. The bio-based sulfone epoxy and modified as well unmodified clay nanocomposites were successfully prepared by using mechanical shearing force and ultrasonication. XRD pattern reveals that the organoclay is delaminated in the epoxy matrix. The morphology of the nanocomposites as studied by SEM and TEM reveals that the clay nanolayers are well distributed in the matrix. Significant enhancement in the performance characteristics of the nanocomposites were observed over the pristine polymer. Further, the impact strength was observed to remain almost constant. The elongation at break and impact strength measurements indicated good flexibility of the synthesized resin and its nanocomposites. Improvements in the thermal stability of the nanocomposites were observed over the neat system. The UL94 and LOI tests

showed significant improvement in the flame retardancy of the nanocomposites compared to the pristine epoxy system. Thus, the resultant system offers a potential high performance material for many advanced applications such as flame retardant, active thin film, surface coating, etc.

References

1. Bergaya, F.; Lagaly, G. Appl Clay Sci 2001, 19, 1.
2. Kaya, E.; Tanoglu, M.; Okur, S. J Appl Polym Sci 2008, 109, 834.
3. Chen, B.; Evans, J. R. G.; Greenwell, H. C.; Boulet, P.; Coveney, P. V.; Bowden, A. A.; Whiting, A. Chem Soc Rev 2008, 37, 568.
4. Pusch, R. In Handbook of Clay Science; Bergaya, F.; Theng, B. K. G.; Lagaly, G., Eds.; Elsevier 2006; Chapter 6, Amsterdam, Netherlands, p 247.
5. Krishnamoorthi, R.; Vaia, R. A.; Giannelis, E. P. Chem Mater 1996, 8, 1728.
6. Giannelis, E. P. Adv Mater 1996, 8, 29.
7. Giannelis, E. P.; Krishnamoorthi R.; Manias, E. Adv Polym Sci 1999, 138, 107.
8. Alexandre, M.; Dubois, P. Mater Sci Eng Rep 2000, 28, 1.
9. Manias, E.; Touny, A.; Wu, L.; Strawhecker, K.; Lu, B.; Chung, T. C. Chem Mater 2001, 13, 3516.
10. Zanetti, M.; Lomakin, S.; Camino, G. Macromol Mater Eng 2000, 279, 1.
11. Vaia, R. A.; Teukolsky, R. K.; Giannelis, E. P. Chem Mater 1994, 6, 1017.
12. Derksen, J. T. P.; Cuperus, F. P.; Kolster, P. Ind Crops Prod 1995, 3, 225.
13. Ahmad, S.; Ashraf, S. M.; Naqvi, F.; Yadav, S.; Hasnat, A. Prog Org Coat 2002, 47, 95.
14. Ikhuoria, E. U.; Aigbodion, A. I.; Okieimen, F. E. Prog Org Coat 2005, 52, 238.
15. Meier, M. A. R.; Metzger, J. O.; Schubert, U. S. Chem Soc Rev 2007, 36, 1788.
16. Pillai, C. K. S.; Prasad, V. S.; Sudha, J. D.; Bera, S. C.; Menon, A. R. R. J Appl Polym Sci 1990, 41, 2487.
17. Dennis, T. J.; Kumar, K. A. Fitoterapia 1998, 69, 291.
18. Konwer, D.; Taylor, S. E.; Gordon, B. E.; Otvos, J. W.; Calvin, M. J Am Oil Chem Soc 1989, 66, 223.
19. Konwar, U.; Karak, N.; Mandal, M. Polym Degrad Stab 2009, 94, 2221.
20. Mahapatra, S. S.; Karak, N. Prog Org Coat 2004, 51, 103.
21. Dutta, S.; Karak, N. Prog Org Coat 2005, 53, 147.
22. Das, G.; Karak, N. Prog Org Coat 2009, 66, 59.
23. Das, G.; Karak, N. Polym Degrad Stab 1948 2009, 94.
24. Das, G.; Karak, N. Prog Org Coat 2010, 69, 495.
25. Kusmono, Z. A.; Ishak, M.; Chow, W. S.; Takeichi, T. Rochmadi, T. Polym Compos 2010, 31, 1156.
26. Madejova, J. Vib Spectrosc 2003, 31, 1.
27. Zhang, Y. Q.; Lee, J. H.; Jang, H. J.; Nah, C. W. Compos B 2004, 35, 133.
28. Kamon, T.; Furakaw, H. In Epoxy Resins and Composites IV, Dusek, K., Ed.; Springer-Verlag: Berlin, 1986, p 177.
29. Lan, T.; Pinnavaia, T. J. Chem Mater 1994, 6, 2216.
30. Chen, B.; Liu, J.; Chen, H.; Wu, J. Chem Mater 2004, 16, 4864.
31. Chiu, Y. C.; Chou, I. C.; Tseng, W. C.; Ma, C. C. M. Polym Degrad Stab 2008, 93, 668.
32. Sikdar, D.; Katti, D. R.; Katti, K. S. Langmuir 2006, 22, 7738.
33. Khanbabaei, G.; Aalaie, J.; Rahmatpour, A.; Khoshniyat, A.; Gharabadian, M. A. J Macromol Sci B 2007, 46, 975.
34. Park, J. H.; Lee, H. M.; Chin, I. J.; Choi, H. J.; Kim, H. K.; Kang, W. G. J Phys Chem Solids 2008, 69, 1375.
35. Li, S. C.; Jarvela, P. K.; Jarvela, P. A. J Appl Polym Sci 1999, 71, 1641.
36. Vlasveld, D. P. N.; Jong, M.; Bersee, H. E. N.; Gotsis, A. D.; Pickena, S. J. Polymer 2005, 46, 10279.
37. Tyan, H. L.; Leu, C. M.; Wei, K. H. Chem Mater 2001, 13, 222.
38. Zhao, C. X.; Zhang, W. D. Eur Polym Mater 1988 2008, 44.
39. Tjong, S. C. Mater Sci Eng R 53:73 2006.
40. Ha, S. R.; Ryu, S. H.; Park, S. J.; Rhee, K. Y. Mater Sci Eng R 2007, 448, 264.
41. Soni, H. K.; Pate1, V. S.; Patel, R. G. Thermochim Acta 1991, 191, 307.
42. Song, R.; Wang, Z.; Meng, X.; Zhang, B.; Tang, T. J Appl Polym Sci 2007, 106, 3488.
43. Jang, B. N.; Costache, M.; Wilkie, C. A. Polymer 2005, 46, 10678.